Cluster Structure and H-Bonding in Native, Substrate-Bound, and 3Fe Forms of Aconitase as Determined by Resonance Raman Spectroscopy

LaTonya K. Kilpatrick,† Mary Claire Kennedy,‡ Helmut Beinert,‡ Roman S. Czernuszewicz,§ Di Qiu,† and Thomas G. Spiro*,†

Contribution from the Department of Chemistry, Princeton University, Princeton, New Jersey 08544, Department of Biochemistry and Biophysics Research Institute, Medical College of Wisconsin, Milwaukee, Wisconsin 53226, and Department of Chemistry, University of Houston, 4800 Calhoun Road, Houston, Texas 77004

Received November 8, 1993®

Abstract: Resonance Raman spectra, with excitation in the visible and near-UV regions, have been investigated for aconitase with and without substrate and inhibitors, using ^{34}S, ^{18}O, and ^{2}H labeling of the active site or substrate. The Fe–O stretching vibrations of bound hydroxide, substrates, or inhibitors are not resonance enhanced. However, their influence is detectable in ^{18}O shifts of FeS modes of the $[Fe_4S^b_4]S^t_3$ cluster and in the frequency elevation of one of the FeS^t modes from ca. 360 to 372 cm^{-1}. The FeS modes have all been assigned. Their frequencies and $^{34}S^b$ shifts are reproduced via normal mode calculations on a cluster model with ethyl thiolate ligands, provided that the FeS–CC dihedral angles are set to the values found in the crystal structures and that allowance is made for FeS force constant differences due to weakening of the bonds to the unique Fe atom, Fe_a, to which OH is attached and strengthening of the bonds to the remaining Fe atoms. The frequencies and isotope shifts are likewise, reproduced for the 3Fe inactive form of aconitase if allowance is made for further strengthening of the bonds to the doubly bridging S atoms, once Fe_a is removed. D_2O shifts of 2 cm^{-1} are seen for the E symmetry FeS^b cluster mode and for an FeS^t mode at 358 cm^{-1} for aconitase with bound substrate, consistent with the H-bonds to both bridging and terminal S atoms deduced from the crystal structure. In native aconitase, the 360-cm^{-1} FeS^t band likewise shifts 2 cm^{-1} in D_2O, and the intensification of this band upon substrate or inhibitor binding indicates an alteration in the excited state of the H-bond interaction with a terminal sulfur atom. In addition, resonance enhancement is observed for amide modes involving C=O stretching (amide I, 1655 cm^{-1}) and C–C–N bending (466 cm^{-1}), identified via their D_2O sensitivity. The 1655-cm^{-1} amide I band shifts to 1642 cm^{-1} when aconitase is dissolved in D_2O, but to 1624 cm^{-1} when it is reconstituted from apoprotein in D_2O. These shifts are consistent with H/D exchange of one and then both protons on a primary amide. It is concluded that the amide modes arise from one or both of the asparagine side chains involved in the H-bonds and that their enhancement arises from electronic coupling with the resonant Fe → S charge-transfer transition via the H-bonds to the cluster.

Introduction

Mitochondrial aconitase is a 83-kDa enzyme that catalyzes the isomerization of citrate to isocitrate through the intermediate *cis*-aconitate during the Krebs cycle (Scheme 1). The active protein contains a diamagnetic $[4Fe–4S]^{2+}$ cluster, while a $[3Fe–4S]^{+}$ cluster is present in the inactive form obtained on isolation.[1-6] Although $[4Fe–4S]^{2+}$ clusters typically participate in electron-transfer reactions, the $[4Fe–4S]^{2+}$ cluster in aconitase directly binds substrate during the catalytic reaction.

Aconitase is the best characterized representative of a relatively new class of Fe–S proteins that catalyze hydrolysis rather than electron-transfer reactions.[7,8] The X-ray crystal structures of substrate-free pig heart aconitase in both the active ($[4Fe–4S]^{2+}$) and inactive ($[3Fe–4S]^{+}$) forms have been solved by Stout and collaborators.[9-12] The crystal structure of active aconitase reveals that one of the iron atoms, "Fe_a" (the labile iron atom released during the $[4Fe–4S]^{2+} \rightarrow [3Fe–4S]^{+}$ conversion), is coordinated to a OH_x (x = 1 or 2) group instead of a cysteine residue, as is typically found in Fe–S clusters. ^{1}H and ^{2}H electron nuclear

Scheme 1

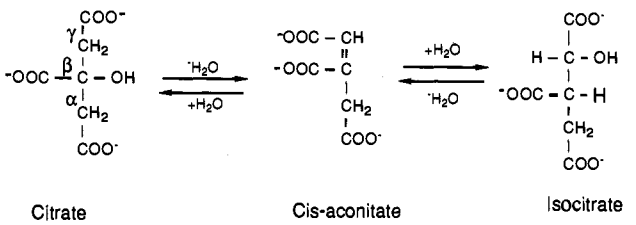

* Author to whom correspondence should be addressed.
† Princeton University.
‡ Medical College of Wisconsin.
§ University of Houston.
® Abstract published in *Advance ACS Abstracts*, April 1, 1994.

(1) Kent, T. A.; Dreyer, J.-L.; Kennedy, M. C.; Huynh, B. H.; Emptage, M. H.; Beinert, H.; Münck, E. *Proc. Natl. Acad. Sci. U.S.A.* **1982**, *79*, 1096–1100.
(2) Kennedy, M. C.; Emptage, M. H.; Dryer, J.-L.; Beinert, H. *J. Biol. Chem.* **1983**, *258*, 11098–11105.
(3) Emptage, M. H.; Dreyer, J.-L.; Kennedy, M. C.; Beinert, H. *J. Biol. Chem.* **1983**, *258*, 11106–11111.
(4) Beinert, H.; Emptage, M. H.; Dreyer, J.-L.; Scott, R. A.; Hahn, J. E.; Hodgson, K. O.; Thomson, A. *J. Proc. Natl. Acad. Sci. U.S.A.* **1983**, *80*, 393–396.
(5) Rydén, L.; Öfverstedt, L.-G.; Beinert, H.; Emptage, M. H.; Kennedy, M. C. *J. Biol. Chem.* **1984**, *259*, 3141–3144.
(6) Johnson, M. K.; Czernuszewicz, R. S.; Spiro, T. G.; Ramsay, R. R.; Singer, T. P. *J. Biol. Chem.* **1983**, *258*, 12771–12774.
(7) Beinert, H.; Kennedy, M. C. *Eur. J. Biochem.* **1989**, *186*, 5–15.
(8) Emptage, M. H. *Metal Clusters in Proteins*; Que, L., Jr., Ed.; ACS Symposium Series 372; American Chemical Society: Washington, DC, 1988; Chapter 17.
(9) Robbins, A. H.; Stout, C. D. *J. Biol. Chem.* **1985**, *260*, 2328–2333.
(10) Robbins, A. H.; Stout, C. D. *Proc. Natl. Acad. Sci. U.S.A.* **1989**, *86*, 3639–3643.
(11) Robbins, A. H.; Stout, C. D. *Proteins: Struct. Funct. Genet.* **1989**, *5*, 289–312.
(12) Werst, M. M.; Kennedy, M. C.; Beinert, H.; Hoffman, B. *Biochemistry* **1990**, *29*, 10526–10532.

0002-7863/94/1516-4053$04.50/0

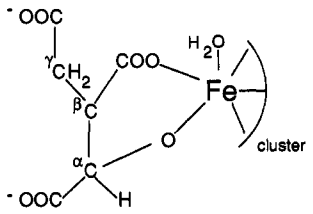

Citrate Bound Cluster

Figure 1. Proposed geometry for citrate binding to the Fe_4S_4 cluster in aconitase.

double resonance (ENDOR) experiments have revealed that the OH_x ligand is actually a hydroxyl group.[12]

The X-ray crystal structures have also been solved for mitochondrial aconitase in the presence of isocitrate and nitroisocitrate[13] or of *trans*-aconitate and nitrocitrate.[14] (Nitroisocitrate is an inhibitor in which the C-2 carboxylate group of the substrate is replaced with a nitro group.) Isocitrate and nitroisocitrate bind to Fe_a through their C-α carboxyl and hydroxyl groups and have identical conformations, while nitrocitrate and *trans*-aconitate model the binding of citrate and *cis*-aconitate, respectively. The structural data are consistent with the previous Mössbauer, electron paramagnetic resonance (EPR), and ^{17}O ENDOR spectroscopic results obtained for the reduced, [4Fe–4S]$^+$ form of aconitase[12,15-19] (a form that is only 30% active.) When isocitrate binds to the cluster, Fe_a moves 0.2 Å away from the corner of the [4Fe–4S]$^{2+}$ cube, but the Fe–S bond lengths are not significantly altered.[13] The spectroscopic findings are consistent with the catalytic mechanism proposed earlier by Gawron et al., in which *cis*-aconitate binds to iron through the C-β carboxylate group, dissociates from the active site, rotates 180°, and reassociates in the orientation necessary to form isocitrate (Figure 1).[20]

Resonance Raman (RR) spectroscopy is capable of detecting structural alterations at chromophoric sites in proteins. In an early application, Johnson et al.[6] used RR spectroscopy to establish structural homology between active and inactive aconitase and other proteins containing [4Fe–4S]$^{2+}$ and [3Fe–4S]$^+$ clusters. In the present work we have carried out a more thorough analysis of the RR spectra of aconitase in a variety of forms, focusing on the effects of (1) hydroxide or substrate/inhibitor binding to Fe_a, (2) cysteine ligand conformational changes, and (3) H-bonding to the cluster from protein donor groups.

Materials and Methods

Sample Preparation. $H_2{}^{18}O$, 99 atom %, and ^{34}S, ≥93 atom %, were obtained from ICON Services Inc., Summit, NJ. ^2H_2O, 99.9 atom %, was obtained from Aldrich Chemical Co., Inc., Milwaukee, WI. Aconitase was prepared and assayed as described previously.[2] ^{18}O labeling of the C-1 carboxyl and hydroxyl groups of nitroisocitrate (1-hydroxy-2-nitro-1,3-propanedicarboxylate) were carried out as described in ref 19. Samples in ^2H_2O and $H_2{}^{18}O$ were prepared according to ref 13. Deuterium-exchanged protein was prepared either by converting the native enzyme to the purple form and reconstituting in ^2H_2O as described in ref 21 or by conversion to the apoprotein followed by reconstitution in ^2H_2O.[16] $Na_2{}^{34}S$- and ^{34}S-enriched enzymes were prepared as indicated in ref 16. In samples containing substrate or inhibitor their concentrations were ~5–10 times the enzyme concentration (~1.0 mM).

Resonance Raman Spectroscopy. Resonance Raman spectra of aconitase were obtained usng a 135° backscattering geometry. The frozen protein was mounted on a copper cold finger cooled with liquid N_2.[22] This sample-handling technique requires very little protein (~25 μL), reduces the incidence of protein photodecomposition, and also improves the resolution of the resulting RR spectrum because of the low temperatures employed. (The protein samples, in 0.1 mM HEPES, pH 7.5, were 1–2 mM in beef heart mitochondrial aconitase and 5–8 mM in substrate or inhibitor.) The RR data obtained for the natural abundance and isotopically labeled enzyme were collected using a Spex 1401 double monochromator. The signal was detected with a cooled Hamamatsu R1220 photon multiplier tube. Slit widths of 4 cm^{-1} were used, and typical laser powers ranged from 100 to 150 nW. To ensure accuracy in the measurement of isotopic shifts, the natural abundance and labeled samples were loaded side by side onto the copper cold finger so that the RR data could be collected under the same conditions. For samples in which isotopic data were not of interest, RR spectra were also obtained using a 1877 Spec triplemate spectrograph with a Princeton Instruments intensified diode array detection system.

All spectra were calibrated using the known vibrational modes of carbon tetrachloride and dimethylformamide. The spectra obtaiend from the scanning double monochromator are the sum of 6–8 scans at 5 s/point and 0.5 cm^{-1}/s increments. Sulfate (~200 mM) was used as the internal standard for the excitation profile measurements. Raman excitation was provided by a Coherent Innova 100-K3 Kr^+ and a Spectra Physics 2025 Ar^+ laser. The RR data weree processed using Lab Calc, a software package from Galactic Industries Corp.

Results and Discussion

Fe–O Stretching Vibrations Are Not Enhanced. An initial objective of this study was to probe the vibrational modes associated with exogenous ligands bound to the FeS cluster. The Fe_a atom is coordinated to hydroxide in the active substrate-free enzyme and to alkoxy and carboxy groups of bound substrate or the inhibitor, nitroisocitrate. It would be of great interest to detect and monitor the Fe–O stretching frequencies associated with these bonds. Such modes are expected to occur in the 400–600-cm^{-1} region, on the bassis of other Fe complexes with hydroxide, alkoxide, or carboxylate ligands.[23-25] This region of the RR spectrum was carefully searched, using samples of aconitase equilibrated with $H_2{}^{18}O$, as well as aconitase with nitroisocitrate bound, which had been labeled with ^{18}O in the carboxyl or hydroxyl positions. No ^{18}O-sensitive bands were detected, however.

These negative findings are not altogether surprising, since the visible absorption spectrum of aconitase is dominated by bands associated with S → Fe charge-transfer transitions. These transitions provide RR enhancement of the vibrations associated with the Fe–S bonds, which are found below 400 cm^{-1}. The absence of detectable enhancement for the Fe–O vibrations implies that the Fe–O bond lengths are not significantly altered in the S–Fe CT excited states. Some extension might have been expected

(13) Lauble, H.; Kennedy, M. C.; Beinert, H.; Stout, C. D. *Biochemistry* **1992**, *31*, 2735–2748.
(14) Lauble, H.; Kennedy, M. C.; Beinert, H.; Stout, C. D. *J. Mol. Biol.*, in press.
(15) Kent, T. A.; Enptage, M. H.; Merkle, H.; Kennedy, M. C.; Beinert, H.; Munck, E. *J. Biol. Chem.* **1985**, *260*, 6871–6881.
(16) Werst, M. M.; Kennedy, M. C.; Houseman, A. L. P.; Beinert, H.; Hoffman, B. M. *Biochemistry* **1990**, *29*, 10533–10540.
(17) Emptage, M. H.; Kent, T. A.; Kennedy, M. C.; Beinert, H.; Münck, E. *Proc. Natl. Acad. Sci. U.S.A.* **1983**, *80*, 4674–4678.
(18) Telser, J.; Emptage, M. H.; Merkle, H.; Kennedy, M. C.; Beinert, H.; Hoffman, B. M. *J. Biol. Chem.* **1986**, *261*, 4840–4846.
(19) Kennedy, M. C.; Werst, M.; Telser, J.; Emptage, M. H.; Beinert, H.; Hoffman, B. *Proc. Natl. Acad. Sci. U.S.A.* **1987**, *84*, 8854–8858.
(20) Gawron, O.; Glaid, A. J., III; Fondy, T. P. *J. Am. Chem. Soc.* **1958**, *80*, 5856–5860.
(21) Houseman, A. L. P.; Oh, B.-H.; Kennedy, M. C.; Fan, C.; Werst, M. M.; Beinert, H.; Markley, J. L.; Hoffman, B. M. *J. Am. Chem. Soc.* **1992**, 2073.
(22) Czernuszewicz, R. S.; Johnson, M. K. *Applied Spectroscopy* **1983**, *37*, 297–298.
(23) (a) Asher, S. A.; Schuster, T. M. *Biochemistry* **1979**, *18*, 5377–5387. (b) Asher, S. A.; Vickery, L. E.; Schuster, T. M.; Sauer, K. *Biochemistry* **1977**, *16*, 5849–5856. (c) Desbois, A.; Lutz, M.; Banerje, R. *Biochemistry* **1979**, *18*, 1510–1518. (d) Hoard, J. L.; Hamor, M. J.; Hamor, T. A.; Caughey, W. S. *J. Am. Chem. Soc.* **1965**, *87*, 2312–2319.
(24) (a) Rodgers, K. R.; Reed, R. A.; Su, Y. O.; Spiro, T. G. *New J. of Chem.*, in press. (b) Reed, R. A.; Rodgers, K. R.; Kushmeider, K.; Spiro, T. G. *Inorg. Chem.* **1990**, *29*, 2881–2883. (c) Rodgers, K. R.; Reed, R. A.; Su, Y. O.; Spiro, T. G. *Inorg. Chem.*, in press. (d) Shiemke, A. K.; Loehr, T. M.; Sanders-Loehr, J. *J. Am. Chem. Soc.* **1986**, *108*, 2437–2443. (e) Sitter, A. J.; Shifflett, J. R.; Terner, J. *J. Biol. Chem.* **1988**, *263*, 13032–13038.
(25) Nakamoto, K. *Infrared and Raman Spectra of Inorganic and Coordination Compounds*; Wiley-Interscience: New York, 1986; Part III.

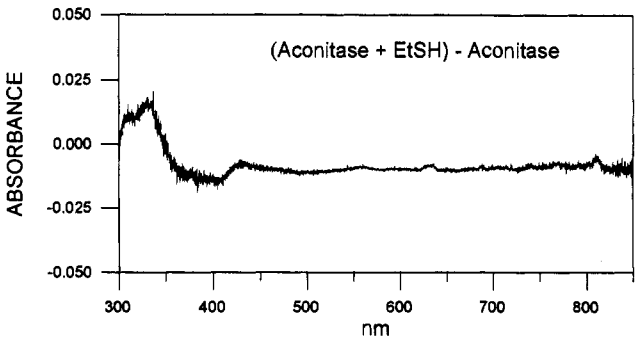

Figure 2. Difference absorption spectrum between native [Fe_4–S_4] aconitase and the ethane thiol-containing enzyme. The spectra of the native enzyme (54 μM) with and without ethane thiol (100 mM) were recorded under anaerobic conditions against a buffer blank (0.10 M HEPES, pH 7.5). Similar results were obtained at twice the enzyme concentration. The peak at 335 nm is due to uncomplexed ethane thiol.

because of the lowered charge on the Fe atoms resulting from the charge transfer. This charge lowering is distributed among all the Fe atoms of the cluster, however, and it is likely that the Fe_a atom, which is bound to the relatively electronegative oxide-derived ligands, participates less in the S–Fe charge transfer than the other three Fe atoms. Fe–O bond stretching is, therefore, unlikely to be significantly involved in the electronic transition.

Enhancement of Fe–O vibrations could be provided by tuning the laser into resonance with O → Fe CT transitions, but the energies of these transitions are uncertain. Thinking that some of them might underlie the dominant S → Fe CT bands, we varied the excitation wavelength over a wide range, from 350 to 680 nm. At none of these wavelengths were ^{18}O-sensitive bands observed in the 400–600-cm^{-1} region. To investigate the issue of O → Fe CT transitions further, we prepared the ethyl thiolate complex of aconitase. On the basis of data obtained from Mössbauer spectroscopy, the bound hydroxide can be displaced by the thiolate in this complex.[26] Consequently, any O → Fe CT transitions must be eliminated. Figure 2 shows the difference absorption spectrum between aconitase and its ethyl thiolate complex. Weak negative bands are seen at 410 and 550 nm, but the difference absorptivities are so small (<300 M^{-1} cm^{-1}) that O → Fe CT assignments are unlikely. Probably these features result from alterations in the distribution of S → Fe CT transitions brought about by the extra thiolate ligand. We therefore surmise that the O → Fe transitions are at energies higher than 350 nm. (Attempts to obtain the RR spectrum of this complex were unsuccessful, perhaps due to instability in the laser beam.)

Effects of OH Binding on Fe–S Cluster Modes. Although the aconitase Fe–OH stretching vibration is not enhanced in the RR spectra, its presence can nevertheless be detected via its interaction with the Fe–S vibrations. Figure 3 shows that RR bands at 392, 372, and 360 cm^{-1} shift down by ca. 1 cm^{-1} when aconitase is equilibrated with $H_2{}^{18}O$, while the 352- and 339-cm^{-1} bands are not shifted. These small downshifts of the highest frequency Fe-S modes are due to vibrational mixing with the (unseen) Fe–O mode, lying at a still higher frequency. In the normal coordinate calculations, to be described below, we obtained ca. 1 cm^{-1} ^{18}OH shifts of the higher frequency Fe–S modes when the Fe–O force constant was set to a value of 1.18 mdyn/Å; the Fe–O frequency was claculated at 408 cm^{-1} with this force constant. Lower values of the force constant gave larger shifts, while higher values gave negligible shifts.

(26) Surerus, K.; Münck, E.; Kennedy, M. C.; Beinert, H. Unpublished results.

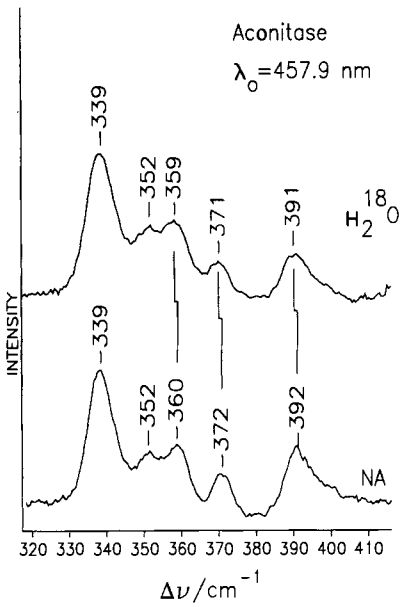

Figure 3. RR spectra (77 K) of natural abundance and $H_2{}^{18}O$-equilibrated (~95% enrichment) native aconitase obtained with 457.9-nm laser excitation (100 mW) and 4-cm^{-1} slit widths. The spectrometer was advanced in 0.5-cm^{-1} increments.

Aside from the isotope shifts occasioned by vibrational mixing, ligation by hydroxide might be expected to have other effects on the Fe–S modes. Replacement of thiolate in the $[Fe_4S_4]S_4$ cluster would lower its maximum symmetry from T_d to C_{3v}, resulting in splittings of triply degenerate modes: $T_2 \rightarrow A_1 + E$, and $T_1 \rightarrow A_2 + E$. In addition, the frequencies should be shifted by the vibrational mixing. To explore these effects, we carried out normal coordinate calculations (Table 1) on a model $[Fe_4S_4]S_4$ cluster. The force field was similar to that used by Czenuszewicz et al.[27] for the model complex $[Fe_4S_4(SCH_2Ph)_4]^{2-}$, but the force constants (Table 2) were brought closer to those reported by Han et al.[28] in the more recent normal mode analysis of Fe_2S_2 clusters. The calculated frequencies and isotope shifts accurately reproduce the RR data for the benzyl cube in solution[27] (column A of Table 1). In this approximation, the ligand atoms beyond S are neglected, and the calculation involves an idealized $[Fe_4S_4]S_4$ cluster with bond distances and angles averaged over those determined in the benzyl cube crystal structure (Table 3). The selective isotope shifts calculated for ^{34}S substitution in the bridging positions show that the modes are readily divided between terminal or bridging Fe–S bond stretches (FeS^t and FeS^b). There are four terminal stretches, grouped into A_1 and T_2 modes, and twelve bridging stretches, grouped into A_1, E, T_1, and two T_2 modes. The two T_2 bridging modes are at the high and low end of the range of frequencies, while the other bridging modes range in between. The terminal modes are found between the higher T_2 and the A_1 bridging modes.

The result of replacing one terminal S atom by hydroxide (point mass 17 amu, K = 1.18 mdyn/Å) is shown in column B of Table 1. For bridging modes, the calculated downshifts are slight (1–2 cm^{-1}). The lowering of the symmetry to C_{3v} splits the T_2 modes into A and E components, and the T_1 components into A_2 and E components. However, the extent of these splittings is calculated to be small enough (1–3 cm^{-1}) that they would not be detected. In the case of the terminal Fe–S stretches, one mode is replaced by the Fe–O stretch. This is allocated to the A_1 mode. At the same time the T_2 mode is split; the E component is left at the parent frequency, 361 cm^{-1}, but the A_1 component rises to 371

(27) Czernuszewicz, R. S.; Macor, K. A.; Johnson, M. K.; Gewirth, A.; Spiro, T. G. *J. Am. Chem. Soc.* **1987**, *109*, 7178–7187.
(28) Han, S. H.; Czernuszewicz, R. S.; Spiro, T. G. *J. Am. Chem. Soc.* **1989**, *111*, 3496–3504.

Table 1. Calculated Frequencies and $^{34}S^b$ Isotope Shifts (cm^{-1}) for Various Models Related to Aconitase (See Text)

T_d	A[a] $Fe_4S^b_4S^t_4$	C_{3v}	B[b] $Fe_4S^b_4S^t_3OH$	C[c] $Fe_4S^b_4(SEt_3)^t_3OH$ 90°	D[d] $Fe_4S^b_4(SEt_3)^t_3OH$ non-90°	E[e] aconitase 90°	F[f] aconitase 90°	G[g] aconitase non-90°	H observed
					Mainly FeS^t				
A_1	386(0)	A_1	371(2)	375(3)	383(1)	364(1)	366(1)	371(1)	372(2)
T_2	362(0)	E	361(0)	364(0)	370(1)	352(1)	355(1)	362(1)	360(1)
					364(0)			354(1)	352(2)
					Mainly FeS^b				
T_2	381(7)	A_1	380(6)	380(6)	379(7)	379(7)	391(7)	391(7)	392(4)
		E	379(7)	380(6)	380(7)	377(7)	389(7)	389(7)	
					380(7)			389(7)	
A_1	336(9)	A_1	334(9)	334(9)	334(9)	334(9)	343(9)	342(9)	339(6)
T_1	280(4)	A_2	282(4)	284(4)	284(4)	281(4)	292(4)	292(4)	299(3)
		E	279(4)	280(4)	280(4)	274(4)	284(4)	286(4)	287(4)
					280(4)			283(4)	
E	262(3)	E	260(3)	261(3)	261(3)	255(1)	268(3)	268(4)	275(4)
					260(3)			267(4)	269(3)
T_2	266(6)	A_1	272(6)	272(6)	272(6)	258(3)	261(5)	264(6)	
		E	266(6)	268(5)	268(5)	259(5)	264(6)	262(5)	
					265(4)			258(5)	255(5)

[a] A: Tetrahedral cluster, using averages of the $(Et_4N)_2[Fe_4S_4(SCH_2Ph_4)_4]$ structural parameters.[40] [b] B: Same as A but with OH (point mass 17 amu) replacing one S^t. [c] C: Same as B but with ethyl groups (point mass 14 amu for CH_2 and 15 amu for CH_3) added to S^t, with 90° FeS–CC dihedral angles. [d] D: Same as C, but with 127°, 94°, and 80° FeS–CC dihedral angles. [e] E: Same as C, but with Fe_aS^b lengthened from 2.31 to 2.35 Å. [f] F: Same as E, but with increased FeS^b force constants (Table 3). [g] G: Same as F, but with dihedrals as in D.

Table 2. Force Constants[a] Used in the Normal Mode Calculation of the $(Fe_4S_4)(SC_2H_5)_3(OH)$ Cube

$K(Fe_a–S^b)^{b,c}$	0.89	$H(S^b–Fe–S^b)$	0.40
$K(Fe–S^b)^c$	0.98	$H(Fe–S^b–Fe)$	0.45
$K(Fe–S^t)^b$	1.21	$H(Fe–S–C)$	0.35
$K(Fe–OH)$	1.18	$H(S–C–C)$	0.82
$K(S–C)$	2.50	$H(S^b–Fe–S^t)$	0.38
$K(C–C)$	4.80	$H(OH–Fe–S^b)$	0.38
		$f(FeS^b–FeS^t)$	0.02
		$f(FeS^b–FeOH)$	0.02
		$f(FeS^b–FeS^b)$	0.02
		$F(Fe\cdots Fe)$	0.12

[a] K stretching (mdyn/Å); H bending (mdyn·Å/rad²); F repulsive gem nonbonded interaction; f stretch–stretch valence interaction (mdyn/Å). S^b and S^t are bridging and terminal sulfurs, respectively. Fe_a refers to the iron atom that is ligated to the hydroxyl ligand. Ethyl related constants are not applicable to calculations in columns A and B of Table 1. K(Fe–OH) is not applicable to column A. [b] For calculation in column E, $K(Fe_a–S^b)$ and K(Fe–S^t) were lowered to 0.82 and 1.21 mdyn/Å (see test) via Badger's rule.[31] [c] $K(Fe_a–S^b)$ was raised to 0.89 mdyn/Å, and the remaining K(Fe–S^b) were raised to 0.98 mdyn/Å for calculations in columns F and G (see text).

Table 3. Structural Parameters for the Normal Mode Calculation[a]

FeS^b	2.31 Å[b]	∠Fe–S–C	99°
$Fe_a–S^b$	2.35 Å[c]	∠S–C–C	114°
Fe–S^t	2.25 Å[b,c]	∠S^b–Fe–S^t	114°
Fe–OH	2.25 Å	∠S^b–Fe–S^b	104°
S–C	1.81 Å	∠S^b–Fe–OH	114°
C–C	1.50 Å	∠Fe–S^b–Fe	74°
		τ(SFe–SC)	180°
		τ(FeS–CC)	80°, 94°, 127° [d]

[a] Ethyl coordinates not applicable to calculations in columns A and B in Table 1; Fe–OH not applicable to calculations in column A. [b] Average values from the $(Et_4N)[Fe_4S_4(SCH_2Ph)_4]$ crystal structure.[40] [c] Average values from aconitase crystal structure,[10] not applicable to calculations in columns A-D. FeS^t is 2.31 Å in aconitase. [d] From aconitase crystal structure; 90° for calculations in columns C, E, and F.

cm^{-1} and also acquires a 2-cm^{-1} $^{34}S^b$ isotope shift by mixing with the A_1 component (380 cm^{-1}) of the T_2 bridging mode. Aside from this effect, the modes remain sorted into terminal and bridging stretches on the basis of the $^{34}S^b$ isotope shifts, as is seen experimentally for aconitase in Figure 4.

These results indicate that the substitution of a single thiolate by hydroxide is not expected to alter the $[Fe_4S_4]S_4$ vibrational pattern significantly, at least not in regard to the bridging modes.

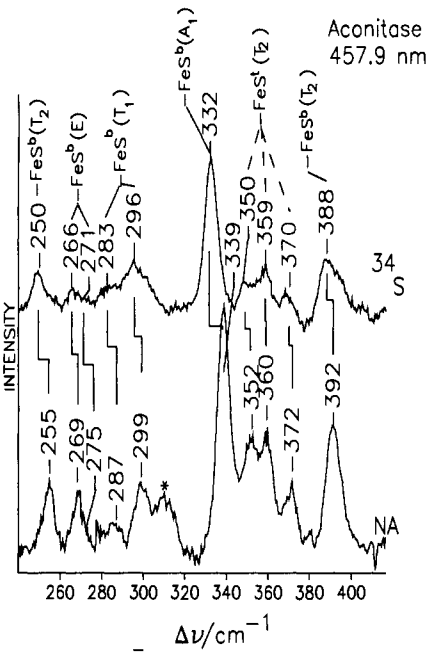

Figure 4. RR spectra (77 K) of natural abundance (NA) and ^{34}S-reconstituted aconitase (1.5 mM, pH = 7.5). Indicated assignments are based on a cluster possessing T_d symmetry. Conditions were the same as in Figure 3. The asterisk marks the position of an ice band.

It is therefore not surprising that the RR spectrum of aconitase resembles those of $[Fe_4S_4]S_4$ proteins and analog complexes rather closely. This similarity is illustrated by the comparison of frequencies and isotope shifts given in Table 4. A unique feature of aconitase, however, is the occurrence of a band at 372 cm^{-1}, which we identify as the A_1 component of the T_2 FeS^t mode. This band is elevated in frequency because the A_1 FeS^t mode is replaced by the higher frequency Fe–OH stretch. The remaining E component is split further, an effect attributable to the cysteine ligand orientations in aconitase, as discussed below.

Another difference is that the FeS^b T_2 mode is at an elevated position, 392 cm^{-1}, in aconitase. The remaining FeS^b modes, however, are very close to those seen in *Clostridium pasteurianum* (*Cp*) and *Clostridium acidi-urici* (*Ca*) ferredoxins[27,29] and also to those of the benzyl cube tetraethylammonium salt,[27] which is known to experience a D_{2d} distortion, with eight long and four short FeS^b bonds. A similar distortion may be imposed by the

Table 4. Vibrational Assignments and Frequencies (cm^{-1}) for Aconitase and Comparison with Ferredoxins from *Clostridium pasteurianum* (*Cp*) and *Clostridium acidi* (*Ca*) and with the Benzyl Cube, $(Et_4N)_2[Fe_4S_4(SCH_2Ph)_4]$

symmetry[a] T_d (C_{3v}/D_{2d})	cube[a,b]	*Cp* ferredoxin[b]	*Ca* ferredoxin[c]	aconitase
		Mainly Terminal ν(Fe–S)		
A_1 (A_1)	391(1)[d]	395(4)	397	372(2)
T_2 (A_1/B_2)	367(1)	351(0.7)	350	352(2)
(E)	359(2)	363(2.0)	366	360(1)
		Mainly Bridging ν(Fe–S)		
T_2 (A_1/B_2)	385(5)	380(5.6)	379	392(4)
(E)				
A_1 (A_1)	335(8)	338(7.0)	339	339(6)
E (E/A_1)	298(5)	298(4.9)	300	299(3)
(E/B_2)	283(4)	276(4.5)	285	287(5)
T_1 (E)	283(4)	276(4.5)	278	275(4)
(A_2)	270(3)	266(4.0)	266	269(3)
T_2 (A_1/B_2)	243(5)			
(E)	249(6)	251(6.2)	255	255(5)

[a] Symmetry labels for an idealized $[Fe_4S_4]S_4$ cube (T_d) and for C_{3v} (aconitase) or D_{2d} (benzyl cube) clusters. [b] Reference 27. [c] Reference 29a. [d] The values in parentheses represent the bridging ^{34}S isotope shifts.

ferredoxin proteins. In the case of aconitase the symmetry is lowered at least to C_{3v} by the OH substituent.

Thiolate Ligand Orientation Effects. The orientation of the thiolate ligands has emerged as an important determinant of the vibrational pattern observed in FeS proteins and analog complexes. Because the natural frequency for SCC bending, ca. 300 cm^{-1},[30] is in the region of the Fe–S stretches, there is potential for significant interaction between the two types of internal coordinates. This interaction is maximal when the dihedral angle about the S–C bond is 180°. In this conformation, the Fe–S stretching and SCC bending coordinates are in line. The interaction is minimal when the dihedral angle is 90°. In [4Fe–4S]$^{2+}$ RR spectra, the occurrence of multiple FeS^t modes near 360 cm^{-1}, where the T_2 mode is expected, has been attributed to these interactions.[27] According to the X-ray coordinates of substrate-free active aconitase,[10] the three cysteinate ligands of aconitase have dihedral angles of 127°, 94°, and 80°. We carried out additional normal coordinate calculations in order to evaluate the influence of this distribution of orientations on the Fe–S modes.

The first step was to add ethyl groups to the terminal sulfur atoms of the $[Fe_4S_4]S_3OH$ complex. Ethyl groups provide the minimum unit to display SCC bending. The SCC bending force constant was taken from the work of Han et al.,[28] and the cluster force constants were left unchanged. Normal Fe–thiolate bond angles were used (99°), and the SFe–SC dihedral angles were set to maintain overall C_{3v} symmetry. Initially, the FeS–CC dihedral angles were set to 90° in order to minimize interactions. The results of this base level calculation are shown in column C of Table 1. The effect of the added ethyl groups is negligible, except for 3–4-cm^{-1} increases in the frequencies of the FeS^t modes. The increase in the FeS^t modes reflects the interactions that exist with the SC stretching vibrations.

Next, the FeS–CC dihedral angles were changed to the values seen in the aconitase crystal structure. The results are shown in column D. The non-90° dihedral angles destroy the C_{3v} symmetry which results in the splitting of the E modes. The degree of splitting is negligible for the bridging modes. But for the terminal modes, which are the primary locus of the FeS/SCC interaction, the E splitting is substantial, 6 cm^{-1}. In addition, the A_1 component of the FeS^t T_2 mode is elevated by 8 cm^{-1}, relative to the 90° dihedral angle model. The net result is that the three terminal modes are now spread out from 364 to 383 cm^{-1} and are separated by intervals of 13 and 6 cm^{-1}. (These effects are mainly determined by the 127° dihedral, which has the most pronounced deviation from 90°. In trial calculations, varying this dihedral by 10° in either direction produced 2–3-cm^{-1} changes in the spread of frequencies.) The predicted pattern of the terminal mode splittings is quite close to the one actually observed in aconitase (Figure 4 and Table 4), except that the frequencies are all ca. 10 cm^{-1} too high. The discrepancy is attributed to the longer Fe–S^t bonds reported for aconitase, 2.33 Å on average, relative to those present in the benzyl thiolate analog, 2.25 Å. No doubt this lengthening arises from the H-bonding to the terminal sulfur atoms which is observed in aconitase (see below). When the force constant is adjusted to this altered length via Badger's rule (Table 2),[31] the predicted frequencies are brought into good agreement with experiment, as discussed below.

Cluster Geometry. The [4Fe–4S]$^{2+}$ cluster is not exactly tetrahedral in aconitase. On average, the three FeS bonds to the OH-bound Fe atom, Fe_a, are slightly longer than the remaining nine FeS bonds, 2.35 Å vs 2.31 Å.[10] This inequivalence is attributable to hydroxide being a stronger σ- and π-donating ligand than sulfide, so that the effective charge on Fe_a is less positive than on the remaining Fe atoms.

We carried out additional normal coordinate calculations to assess the effect of this inequivalence on the vibrational pattern. Starting with the $[Fe_4S_4](SEt)_3(OH)$ C_{3v} model of column C in Table 1, in which all Fe–S bond lengths are 2.31 Å, we lengthened the Fe_a–S bonds to 2.35 Å and adjusted the force constant using Badger's rule (Table 2). The FeS^t force constant was also adjusted at this point to reflect the longer FeS^t distance, mentioned above, in aconitase (Table 2). The result of this calculation is given in column E. The main effect of lowering the Fe_a–S force constant is to lower the components of the lower T_2 bridging mode by 7–14 cm^{-1}. Surprisingly, the upper T_2 frequencies are nearly unaffected, and the A_1/E splittings remain small, despite the pronounced C_{3v} distortion of the cube. The FeS^t frequencies are also lowered, by 8–11 cm^{-1}.

When the frequencies from this calculation are compared with the actual aconitase frequencies (column H), it is apparent that the calculated frequencies are systematically too low, the discrepancies being largest for the upper T_2 bridging frequencies. These discrepancies can be eliminated by raising the FeS^b force constants from 0.82 to 0.89 mdyn/Å for the three bonds to Fe_a and from 0.90 to 0.98 mdyn/Å for the other nine bonds, as shown in column F. The higher force constants are predicted by Badger's rule to shorten all the Fe–S^b bonds by 0.03 Å, an increment that is within the uncertainty of the protein crystallographic determination.

Finally, the dihedral angles were adjusted to the aconitase values, resulting in the calculated frequencies and isotope shifts shown in column G. All of these values are within experimental error of the band positions and shifts seen for aconitase (Figure 4 and column H). Table 1 shows that it is possible to model the aconitase spectrum starting with a tetrahedral cluster and systematically modifying it to resemble the aconitase active site by (1) replacing a terminal thiolate with OH, (2) lengthening the FeS^b bonds, consistent with the protein H-bonding environment, (3) stretching the Fe_a–S^b bonds relative to the other FeS^b bonds, consistent with polarization by the bound OH, and (4) adding ethyl substituents in place of the S^t atoms with FeS–CC dihedral angles the same as those present in the protein.

Substrate and Inhibitor Binding. When the inhibitor nitroisocitrate is bound to aconitase, a dramatic change is seen in the RR spectrum, as shown in Figure 5. Whereas the strongest

(29) (a) Backes, G.; Mino, Y.; Loehr, T. M.; Meyer, T. E.; Cusanovich, M. A.; Sweeney, W. V.; Adman, E. T.; Sanders-Loehr, J. *J. Am. Chem. Soc.* **1991**, *113*, 1237–1245. (b) Mino, Y.; Loehr, T.; Wada, K.; Matsubara, H.; Sanders-Loehr, J. *Biochemistry* **1987**, *26*, 8059–8065.

(30) Durig, J. R.; Bucy, W. E.; Wurrey, C. J.; Carreira, L. A. *J. Phys. Chem.* **1975**, *79*, 988–993.

(31) Badger's rule: $k = 1.86(r_e - d_{ij})^{-3}$, where k is the force constant of the stretching bond, r_e is the bond length at equilibrium, the constant d_{ij} has a fixed value (0.86 for Cu and S) for bonds between atoms from rows i and j of the periodic table. Badger, R. M. J. *Chem. Phys.* **1934**, *2*, 128. Herschbach, D. R.; Laurie, V. W. *J. Chem. Phys.* **1961**, *35*, 458.

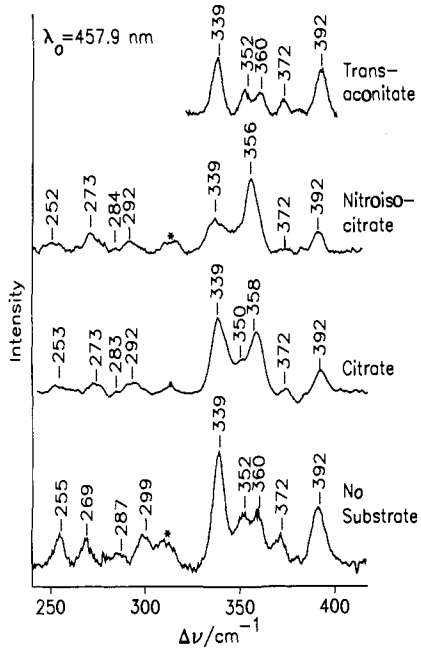

Figure 5. RR spectra (77 K) of aconitase, and after addition of citrate, nitroisocitrate, and *trans*-aconitate obtained with 457.9-nm excitation. The citrate and inhibitor concentrations were between 5 and 8 mM, and the enzyme concentration was between 1 and 2 mM. The RR spectra of the enzyme after addition of nitroisocitrate and citrate were collected using a optical multichannel analyzer (OMA) detector, while the spectra with *trans*-aconitate and without substrate were obtained as in Figure 3. An asterisk marks an ice band.

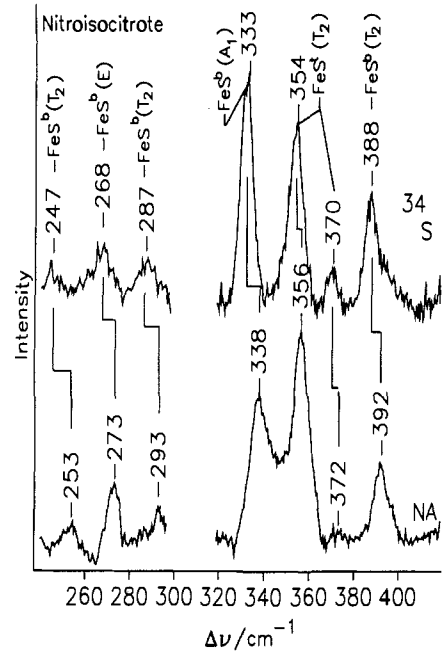

Figure 6. RR spectra (77 K) of natural abundance and ^{34}S-labeled aconitase with nitroisocitrate bound, obtained with 457.9-nm excitation (100 mW) and 4-cm^{-1} slit widths. Spectral assignments are as in Figure 4.

band of the substrate-free protein is the cluster breathing mode at 339 cm^{-1}, the dominant feature of protein with inhibitor bound is a new band at 356 cm^{-1}, which appears to replace the two terminal stretches of the free protein at 352 and 360 cm^{-1}. Noticeable frequency shifts are also observed in the bands below 300 cm^{-1}, but the 372- and 392-cm^{-1} bands are unshifted.

When citrate is added to the enzyme, the RR spectrum is intermediate between the spectra of enzyme with and without inhibitor (Figure 5). In fact, superposition of these two spectra produces a synthetic spectrum resembling that of the citrate-containing enzyme solution quite closely. With substrate present, the enzyme turns over, and the active site contains a mixture of citrate, *cis*-aconitate, and isocitrate (Scheme 1); in addition, product release leaves the active site partially unoccupied. In a freeze–quench Mössbauer experiment, 20% of the signal was found to be characteristic of substrate-free protein,[15] but the fraction of unoccupied sites no doubt varies with conditions. The simplest interpretation of the RR spectrum is that about half of the sites are unoccupied under our conditions and that any of the three interconverting substrates produce a signal characteristic of enzyme with inhibitor bound. Since there is no independent estimate of the site occupancy, however, it cannot be ruled out that only one, or perhaps two, of the three forms produces the same signal as nitroisocitrate and that the signal in the absence of substrate is unaltered by the remaining form(s). It may be that the protein conformation change associated with the nitroisocitrate binding comes into play at the point where citrate is converted to *cis*-aconitate or where *cis*-aconitate is converted to isocitrate. Consistent with this interpretation is the finding (Figure 5) that addition of *trans*-aconitate does not alter the RR spectrum, although this molecule is known to bind and inhibit the enzyme.[18]

What produces the alteration in the RR spectrum upon nitroisocitrate binding? To answer this question, we examined the RR spectrum of enzyme containing ^{34}S at the cluster bridges with bound inhibitor. As seen in Figure 6, the pattern of ^{34}S shifts does not differ materially from that of the free enzyme spectrum (Figure 4). The cluster modes all show shifts in excess of 4 cm^{-1}, while the terminal modes show no more than 2 cm^{-1} shifts. The 338-cm^{-1} band, although not as prominent as in the free enzyme spectrum, is still the cluster breathing mode, while the new band at 356 cm^{-1} is clearly associated with the stretching of terminal bonds. In the RR spectrum of enzyme with substrate, this band (observed at 358 cm^{-1}) is asymmetric, and a shoulder is apparent on the low-frequency side. The shoulder is presumably the third T_2 component. The 356-cm^{-1} (358 cm^{-1} in substrate-containing enzyme) band is therefore assigned to a component of the T_2 FeS^t mode which is intensified relative to inhibitor-free aconitase and downshifted by 4 cm^{-1}, so that it obscures the neighboring T_2 component at 352 cm^{-1}.

This downshift is probably associated with alterations in the S–C dihedral angles of the cysteine ligands, since, as discussed above, these dihedrals determine the distribution of terminal stretching frequencies. The crystal structures show that the range of these dihedrals does narrow upon inhibitor binding; the values for the three cysteine ligands are 80°, 94°, and 127° for Cys-421, 358, and 424 in the free enzyme,[10] whereas the corresponding angles are 100°, 120°, and 100° in the enzyme with nitroisocitrate bound.[13] To investigate the expected effect of these angle changes on the mode frequencies, we carried out an additional calculation, in which the force constants were held at the free enzyme values (column G of Table 1), but the dihedrals were changed to the values when nitroisocitrate is bound. The main result, shown in Table 5 (column A) is a narrowing of the difference between the two lower components of the T_2 FeS^t mode, from 8 to 4 cm^{-1}, consistent with experiment.

The reason for the high intensity of the 356-cm^{-1} band is uncertain. There is evidently a change in the excited-state structure resulting in an increased displacement along the coordinate of this T_2 component. Analysis of this effect will require detailed consideration of electronic interactions at the active site.

The 3Fe Inactive Enzyme. Aconitase is readily converted to an inactive form, in which Fe_a is lost. The RR spectrum of this $[3Fe–4S]^+$-containing protein is shown in Figure 7. It agrees with the previously reported spectrum of this species and with the

Table 5. Calculated Frequencies and $^{34}S^b$ Isotope Shifts for the Aconitase–Nitroisocitrate Adduct[a] and for Inactive Fe_3S_4 Aconitase

A $Fe_4S^b_4(S^tEt_3)_3(OH)$[b]	B observed	C_{3v}	C $Fe_3S_4(SEt_3)$	D observed
	Mainly FeS^t			
369(1)	372(2)	A_1	375(2)	372(1)
361(1)	356(2)	E	353(2)	359(0)
357(1)				
	Mainly FeS^b			
391(7)	392(4)	A_1	402(7)	400(4)
389(7)	382(–)	E	373(5)	
389(7)				
343(9)	338(5)	A_1	345(8)	342(8)
268(3)	273(5)	E	268(3)	264(5)
267(5)				
292(4)	293(6)	A_2	291(4)	
286(4)		E	274(4)	293(4)
283(4)				
264(5)	253(6)			
262(5)				
258(5)				

[a] The model used was the same as that used for column G of Table 1, with FeS–CC dihedral angles changed to 100°, 100°, and 120°. [b] The model used for column G of Table 1 was altered by (1) changing the FeS–CC dihedral angles to 80°, 94°, and 124°, (2) removing Fe_a, and (3) increasing the FeS^b force constant for the six bonds to the doubly bridging S^b atoms to 1.15 mdyn/Å.

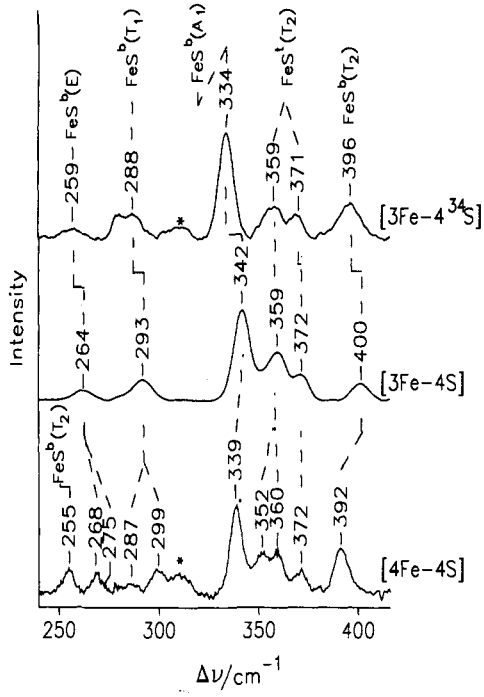

Figure 7. RR spectra (77 K) of the $[3Fe–4S]^+$ inactive aconitase and its ^{34}S isotopomer, compared to active $[4Fe–4S]^{2+}$ aconitase. The RR spectrum of the inactive enzyme was obtained with 488.0-nm laser excitation, while the RR spectrum of the active enzyme was taken with 457.9-nm excitation.

spectra of other $[3Fe–4S]^+$-containing proteins.[32] These spectra resemble those of $[4Fe–4S]^{2+}$-containing proteins, except for a general upshift of cluster modes, especially the ca. 340 and 390 cm^{-1} A_1 and T_2 modes. The lowest T_2, FeS^b mode (255 cm^{-1}) is lost, reflecting the loss of the three FeS^b bonds to Fe_a. These spectra were analyzed in some detail at a time when there was uncertainty whether the 3Fe centers were Fe_3S_3 rings or $[4Fe–4S]^{2+}$ cubes with the corner removed, as was subsequently established crystallographically. The RR spectra were shown to be consistent with the latter structure and inconsistent with the former.[32] An attempt to calculate the frequencies was only partially successful, however, since the cluster modes were calculated to be lower than in the parent $[4Fe–4S]^{2+}$ cluster, rather than higher.

This calculated downshift is a kinematic consequence of the loss of the three Fe_aS bonds. The remaining FeS^b stretches arrange themselves into modes that fall at lower frequencies, on average, than those of the parent $[4Fe–4S]^{2+}$ cluster. To raise these frequencies, the FeS^b force constants have to be increased. In Table 5, we show that it is straightforward to calculate the $[3Fe–4S]^+$ frequencies and $^{34}S^b$ isotope shifts satisfactorily by the simple expedient of selectively raising the stretching force constants for the doubly bridging S^b atoms, from which the Fe_a atom has been removed. The results in column C were obtained by (1) starting with the ethyl cube model of native aconitase in column G of Table 1, (2) rotating the FeS–CC dihedral angles to the values found in the crystal structure of 3Fe aconitase[10] (80°, 94°, 124°), (3) removing Fe_a and its OH ligand, and (4) raising the stretching force constant for the six doubly bridging FeS^b bonds to 1.15 mdyn/Å, while leaving the constant for the three triply bridging FeS^b bonds at the previous value of 0.98 mdyn/Å. It is physically reasonable to incease the doubly bridging FeS^b force constants because the removal of Fe_a increases the negative charge on S^b, thereby strengthening the remaining FeS^b bonds. Application of Badger's rule[31] predicts an associated FeS^b bond contraction of 0.07 Å.

Hydrogen Bonding. Hydrogen bonding is a common motif in Fe–S proteins. Protein crystallography frequently locates –XH groups in a favorable position to donate H-bonds to bridging or terminal sulfur atoms, thereby stabilizing the negative charge on the Fe–S complex. H-bonding modulates the redox potential. It has been noted that bacterial ferredoxins, whose 4Fe clusters are reducible from the $[4Fe–4S]^{2+}$ to the $[4Fe–4S]^+$ level, have more –XH···S H-bonds than does high-potential Fe–S protein (HiPiP), whose 4Fe cluster is instead oxidizable from the $[4Fe–4S]^{2+}$ to the $[4Fe–4S]^{3+}$ level.[29a,32–35] The aconitase X-ray structure locates two asparagine residues with side chains in a favorable position to form NH···S H-bonds: Asn-446 to a bridging S atom of the cluster (N···S = 3.43 Å, ∠N–H···S = 171°) and Asn-258 to a terminal S atom of Cys-358 (N···S = 3.28 Å, ∠N–H···S = 159°). When substrate is bound,[13] a third H-bond forms, this time from the amide NH group of the Cys-358 residue to another bridging S atom of the cluster (N···S = 3.33 Å, ∠N–H···S = 149°).

When Fe–S proteins are dissolved in D_2O, some of the Fe–S stretching RR bands undergo slight but measurable frequency shifts, a phenomenon that has been attributed to the effect of H/D substitution on the –XH···S H-bonds and indirectly on the FeS bond strength.[29] Figure 8 shows this effect on the RR spectrum of aconitase with substrate bound. The 273-cm^{-1} FeS^b band and the 359-cm^{-1} FeS^t band shift down 2 cm^{-1} in D_2O, while the remaining FeS bands are unshifted. This observation is consistent with selective effects of the H-bonds formed with the bridging and terminal S atoms, respectively. It also suggests that the 359-cm^{-1} mode has a large contribution from the S^t atom of Cys-358, since this is the sole S^t atom to receive a H-bond. The corresponding FeS^t band in native aconitase, 360 cm^{-1}, also shifts down 2 cm^{-1} in D_2O, as shown in Figure 9, consistent with the S^t atom of Cys-358 remaining involved in the H-bond. One can speculate that the reason for the intensification of this band upon binding substrate is that the H-bond strength changes more in the Fe–S charge-transfer excited state, because of an alteration in the disposition of polar groups in the neighborhood of the Cys-358 side chain.

(32) (a) Johnson, M. K.; Czernuszewicz, R. S.; Spiro, T. G.; Fee, J. A.; Sweeney, W. V. *J. Am. Chem. Soc.* **1983**, *105*, 6671–6678. (b) Sweeney, W. V.; Rabinowitz, J. C. *Ann. Rev. Biochem.* **1980**, *49*, 139–161.

(33) Adman, E. T.; Watenpaugh, K. D.; Jensen, L. H. *Proc. Natl. Acad. Sci, U.S.A.* **1975**, *72*, 4854–4858.

(34) Sheridan, R. P.; Allen, L. C.; Carter, C. W., Jr. *J. Biol. Chem.* **1981**, *256*, 5052–5057.

(35) Carter, C. W., Jr. *J. Biol. Chem.* **1977**, *252*, 7802–7811.

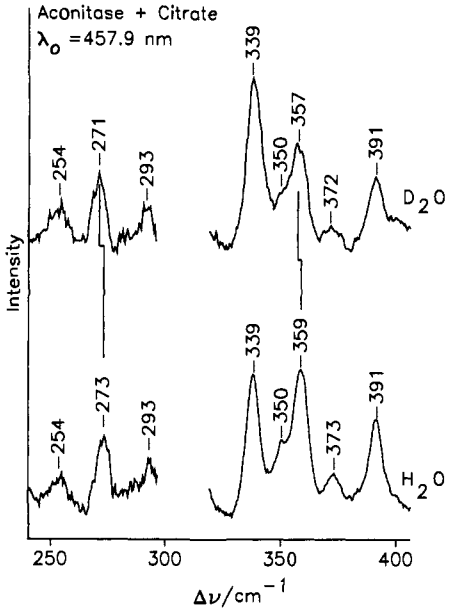

Figure 8. RR spectra (77 K) of aconitase after addition of citrate and equilibrated in H_2O and D_2O. The spectra were obtained with 457.9-nm laser excitation (100 mW) and 4-cm^{-1} slit widths. The spectrometer was stepped in 0.5-cm^{-1} increments.

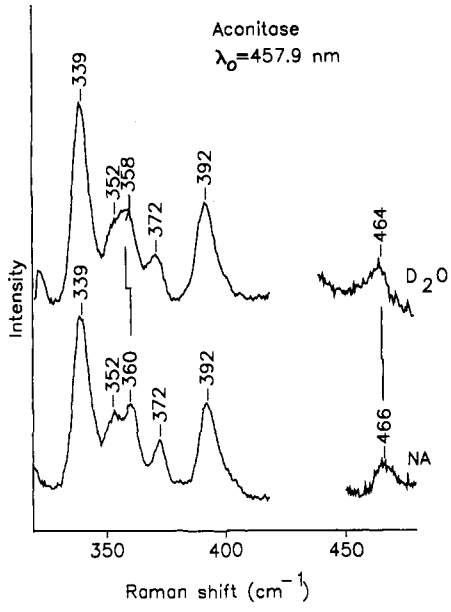

Figure 9. RR spectra (77 K) of native aconitase equilibrated with H_2O and D_2O, obtained with 457.9-nm laser excitation. Conditions are as in Figure 8.

The 273-cm^{-1} band of aconitase with substrate bound is assigned to the E FeS^b cluster mode (Table 5). In the native aconitase spectrum (Figure 4), this band is broad and has two components, reflecting a 6-cm^{-1} splitting of the E mode. (For this reason the D_2O shift could not be reliably determined.) This splitting was not reproduced in any of our model calculations (Table 1). It is possible that the splitting is itself a result of the NH···S^b H-bond, which induces asymmetry in the cluster. The loss of this splitting in aconitase with bound substrate (Figure 8) might then result from the additional NH···S^b H-bond shifting the E components back together and reducing the apparent asymmetry.

An additional D_2O-sensitive band was found in the native aconitase RR spectrum, at 466 cm^{-1} (Figure 9). This frequency is too high for an FeS mode, but is in the region where C–C–N

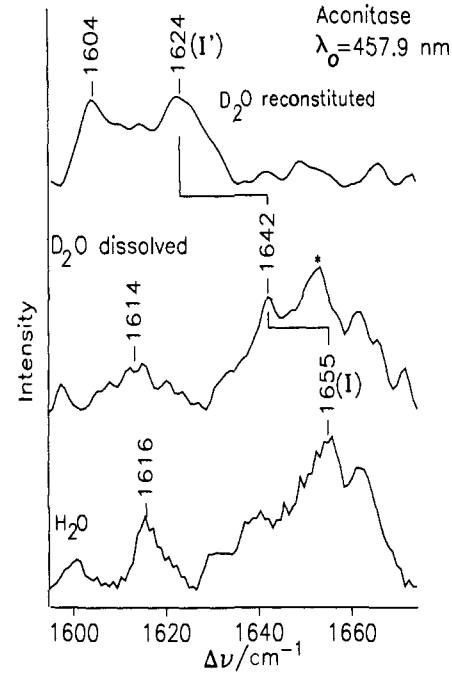

Figure 10. RR spectra (77 K) obtained with 413.1-nm laser excitation in the amide I region of aconitase in H_2O and dissolved or reconstituted (see text) in D_2O. The peak marked with an asterisk in the second spectrum is attributed to residual unexchanged amide groups. All spectra were collected using a triplemate/intensified diode array spectrometer system.

bending modes of peptides are found.[36,37] These modes are found to shift by ca. 2 cm^{-1} upon amide NH/D exchange, the same shift observed for aconitase. Strikingly, an amide I (C=O stretching) band, at 1655 cm^{-1}, was also observed with 457.9-nm excitation, as seen in Figure 10. This band shifted to 1642 cm^{-1} when aconitase was dissolved in D_2O, but to 1624 cm^{-1} when the $[4Fe\text{–}4S]^{2+}$ cluster was reconstituted from apoaconitase in D_2O. These are the expected shifts for the amide I mode of a primary amide group when one and then two of the NH_2 protons are exchanged for deuterons.[38,39] This experiment establishes that the 1655-cm^{-1} band does not arise from the backbone amide bonds of the protein but from a primary amide side chain. Furthermore, the 1655-cm^{-1} band is resonance enhanced via a S → Fe charge-transfer transition of the chromophore. Resonance enhancement was established with the excitation profile shown in Figure 11. The intensity of the 1655-cm^{-1} band was measured relative to the 982-cm^{-1} band of sulfate ion, added as an internal standard, at a series of visible–near UV wavelengths. The intensity reached a maximum at 488.0 nm, near the maximum of the S → Fe charge-transfer absorption band, and fell off on either side.

We therefore assign the 1655-cm^{-1} band to the amide I mode of the Asn-446 and/or the Asn-258 side chains, which are H-bonded to S^b and S^t atoms, respectively, of the chromophore. Dissolving aconitase in D_2O exchanges only one of the protons of the primary amide group(s), as expected, since the other proton is involved in the H-bond and is therefore protected from exchange. Reconstitution from apoprotein, however, renders both protons exchangeable. (The assignment of another D_2O-sensitive band at 1616 cm^{-1} (Figure 10) is uncertain. This band is in a region where Phe and Tyr ring modes are expected, but the frequencies

(36) Hirakawa, A.; Hirakawa, A. Y.; Tsuboi, M. *J. Mol. Spectrosc.* **1984**, *108*, 206–214.
(37) Jakes, J.; Krimm, S. *Spectrochim. Acta* **1971**, *27A*, 35–63.
(38) Tu, A. T. *Spectroscopy of Biological Systems*; Clark, R. J. H., Hester, R. E., Eds.; John Wiley & Sons Ltd: New York, 1986; Chapter 2.
(39) Carmona, P.; Molina, M.; Martinez, P.; Altabef, A. B. *Appl. Spectrosc.* **1991**, *45*, 977–982.
(40) Averill, B. A.; Herskovitz, T.; Holm, R. H.; Ibers, J. A. *J. Am. Chem. Soc.* **1973**, *95*, 3523–3534.

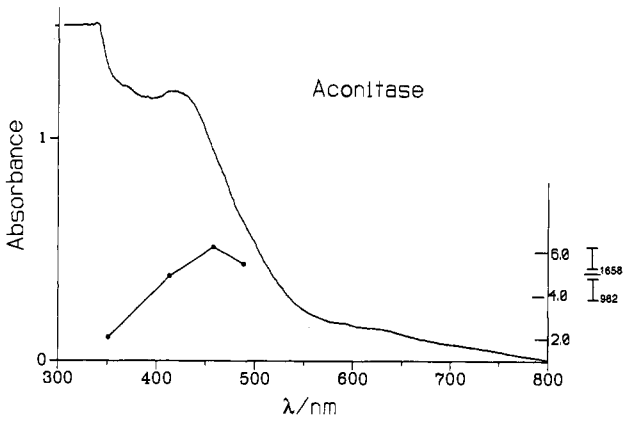

Figure 11. Raman excitation profile for the 1655-cm^{-1} amide I Raman band (●) of aconitase superimposed on the absorption spectrum (~0.1 mM protein). SO_4^{2-} (~200 mM) was used as the internal standard. The RR intensities were measured with 350.7-, 413.1-, 457.9-, and 488.0-nm excitation.

of these modes are not sensitive to D_2O. Conceivably, D_2O alters the relative intensities of ring modes of different residues, producing an apparent frequency shift.)

This is the first example of resonance enhancement of an internal vibrational mode of a group that is H-bonded to a chromophore. Evidently, the H-bond is sufficiently coupled to the S → Fe charge-transfer transition that the excited state involves a significant displacement along the C=O stretching coordinate of the H-bonded amide, as well as along the C–C–N coordinate (466-cm^{-1} band). Further evidence of this electronic interaction comes from recent ENDOR experiments which identified ^{14}N and ^{2}H signals, coupled to the unpaired electron on the FeS cluster of reduced aconitase.[21] These signals no doubt involve the same Asn residue(s) that give rise to the 1655-cm^{-1} RR band.

Conclusions

The Fe–O stretching vibrations of native aconitase or of bound substrates or inhibitors are not directly detectable in RR spectra, but they do induce detectable ^{18}O shifts in the higher frequency FeS modes, via kinematic coupling. In addition, the existence of these bonds elevates one component of the T_2 FeS^t stretching mode to 372 cm^{-1}, a uniquely high frequency in relation to $[Fe_4S^b_4]$-S^t_4 clusters. The terminal mode frequencies for aconitase, with and without substrate, are satisfactorily modeled with ethyl thiolate ligands if the crystallographically determined FeS–CC dihedral angles are used. The bridging mode frequencies and isotope shifts can be reproduced provided the weakening of the FeS bonds to Fe_a and the strengthening of the bonds to the remaining Fe atoms are taken into account. The band frequencies of the inactive $[Fe_3S_4]S_3$ protein can likewise be reproduced, if the doubly bridging FeS bonds are further strengthened, as expected upon removal of Fe_a.

H-bonding to two bridging S atoms is responsible for D_2O sensitivity of the 273-cm^{-1} E mode of the cluster in substrate-bound aconitase, and loss of one of these H-bonds in native aconitase may be responsible for splitting the E mode into two components. H-bonding to the S atom of the Cys-358 ligand produces a selective D_2O shift of the 360-cm^{-1} terminal FeS stretch and may be responsible for its intensification upon substrate binding. One or both of the H-bonds from the Asn-446 and Asn-258 side chains produce resonance enhancement of the primary amide C=O stretching and C–C–N bending modes, reflecting significant electronic coupling of the H-bond(s) to the S → Fe charge-transfer transition.

Acknowledgment. This work was supported by NIH Grants GM 13498 (to T.G.S.) and GM 34812 (to H.B.).